land

MDPI

Article

SVM-GAM Downscaling Framework for Quantifying Ecological Losses in Data-Limited Estuarine Dredging Areas

Zijing Liu [1,2], Zhaoxing Han [1,2,3,*], Liguo Zhang [1,2], Dingkun Yin [1,2], Jinxiang Cheng [1,2], Ning Zhang [1,2], Shengqiang Liu [1,2], Chaohui Zheng [1,2], Jie Liu [1,2], Yue Li [1,2], Jinpeng Lv [1,2], Qi Liu [1,2] and Junhui He [4,5]

[1] Transport Planning and Research Institute, Ministry of Transport, Beijing 180081, China; liuzijing@tpri.org.cn (Z.L.); zhanglg@tpri.org.cn (L.Z.); yindingkun@tpri.org.cn (D.Y.); chengjx@tpri.org.cn (J.C.); zhangning@tpri.org.cn (N.Z.); liusq@tpri.org.cn (S.L.); zhengch@tpri.org.cn (C.Z.); liujie@tpri.org.cn (J.L.); liyue@tpri.org.cn (Y.L.); lvjp@tpri.org.cn (J.L.); liuqi@tpri.org.cn (Q.L.)
[2] Laboratory of Transport Pollution Control and Monitoring Technology, Transport Planning and Research Institute, Ministry of Transport, Beijing 100028, China
[3] School of Environment, Tsinghua University, Beijing 100084, China
[4] Pinglu Cannal Group Co., Ltd., Nanning 530000, China; hejunhui925@163.com
[5] Guangxi Laboratory of Modern Canal, Nanning 530011, China
* Correspondence: hanzx19@mails.tsinghua.edu.cn

Abstract

Accurate quantification of ecological losses in estuarine environments is often hindered by the mismatch between coarse-resolution biological surveys and fine-scale physical disturbances from engineering activities. While numerical models can simulate high-resolution environmental shifts, the inherent sparsity of ecological monitoring points limits the precision of spatial impact assessments. This study develops an integrated spatial-downscaling framework to transform sparse monitoring data into a high-resolution spatial continuum. A three-tiered modeling approach was used: first, the estuarine domain was partitioned into five eco-hydrodynamic zones using an entropy-weighted Support Vector Machine (SVM); second, localized chained Generalized Additive Models (GAMs) were established within each zone using MIKE-simulated hydrodynamic and water-quality data as proxy drivers; and third, these localized response functions were propagated across the study area to quantify multi-trophic biomass and economic losses. The framework revealed substantial spatial non-stationarity. Dredging operations locally altered the estuarine hydrodynamic regime. In northern channels, decreases in flow velocity were statistically associated with phytoplankton biomass to decline by 5.0% to 23.42%. Conversely, southern velocity increases enhanced water exchange and plankton growth. Using silt curtains as a mitigation strategy reduced the loss of phytoplankton by 11.4% and zooplankton by 9.6%. As a result, the total economic loss decreased from 26.54 million CNY to 25.34 million CNY, equivalent to a 4.5% reduction in economic loss. These results indicate that the proposed downscaling method can generate spatially explicit biological estimates. By offering a systematic pathway for impact evaluation and compensation in data-limited coastal regions, this framework supports more ecologically sustainable dredging operations. Nevertheless, the framework remains dependent on the representativeness of sparse monitoring stations, and future applications should integrate cross-estuary validation to improve transferability and uncertainty control.

Keywords: spatial downscaling; dredging impacts; ecological loss quantification; support vector machine; generalized additive model; estuarine ecosystem

Check for updates

Academic Editor: Mattia Iannella

Received: 7 May 2026
Revised: 18 June 2026
Accepted: 23 June 2026
Published: 3 July 2026

Copyright: © 2026 by the authors. Licensee MDPI, Basel, Switzerland. This article is an open access article distributed under the terms and conditions of the Creative Commons Attribution (CC BY) license.

1. Introduction

Estuarine and coastal areas reflect dynamic environments where complex hydrological–biological interactions may be disrupted by engineering projects [1]. Dredging is a key engineering activity for maintaining navigational safety, developing infrastructure, and supporting maritime trade. Resuspended sediment (SS) from dredging increases turbidity and can inhibit phytoplankton photosynthesis [2]. It can also impair respiratory and feeding structures in zooplankton and fish [3–5]. To promote environmentally friendly dredging methods, it is important to measure these effects [3,6]. Traditional quantitative assessments of engineering impacts on ecosystems often use monitoring data [7]. However, a limited number of discrete sampling sites frequently constrain ecological monitoring in these regions [8]. When extending localized point-source data to larger engineering impact zones, this intrinsic data sparsity creates uncertainty because point observations cannot reflect the spatial variability of the entire water body [8–10]. A key limitation of traditional methods lies in the mismatch between coarse-resolution biological surveys and the fine-scale environmental gradients induced by dredging. Previous studies have assessed estuarine engineering impacts using hydrodynamic, water-quality, ecological monitoring, and statistical approaches. Hydrodynamic and sediment-transport models have been widely used to simulate tidal-current changes and suspended-sediment dispersion related to dredging or channel construction [11,12]. Field monitoring and biological community assessments provide direct ecological evidence, but their spatial representation is often limited by the number and distribution of sampling stations [13,14]. Statistical and machine-learning methods can support environmental classification and spatial prediction under data-limited conditions [15]. However, physical models usually focus on hydrodynamic or water-quality processes, whereas monitoring-based assessments may not fully describe spatially continuous disturbance fields. Therefore, linking high-resolution physical simulations with limited biological observations may provide a practical framework for assessing spatial ecological impacts in estuarine engineering projects. To overcome the limitations of sparse monitoring data, there is a need for a robust data downscaling mechanism. Downscaling in this context refers to the process of using high-resolution environmental variables as drivers to reconstruct high-resolution biological surfaces from limited sampling points [16,17]. While machine-learning techniques such as Support Vector Machines (SVM) and Random Forests have been applied in various geographic fields for spatial interpolation, their application in cascading ecological modeling within complex estuaries remains underdeveloped. The primary challenge is not solely spatial interpolation but also the development of localized frameworks [10,18]. Conventional linear models fail to adequately represent the intricate, site-specific responses exhibited in estuarine ecosystems affected by engineering disturbances [7,19]. To tackle this issue, sophisticated statistical and modeling methodologies, including Generalized Additive Models (GAMs), have increasingly been used. GAMs enable flexible, nonparametric modeling of ecological responses to various covariates and have demonstrated efficacy in forecasting biomass and distribution patterns of aquatic organisms amid fluctuating environmental conditions [7]. Similar limitations have been reported in several estuarine and coastal monitoring studies. For example, in the San Francisco Bay–Delta Estuary, water-quality monitoring relies largely on fixed monitoring stations, whose limited spatial coverage can hinder the interpretation of spatially heterogeneous water-quality patterns [20,21]. Comparable station-based ecological studies have also been conducted in the Sado Estuary, Portugal, where four stations across three estuarine regions were used to assess phytoplankton dynamic [22], and in the Tagus Estuary, Portugal, where previous studies were reported to have focused mainly on the upper estuary rather than the whole system [23]. These examples indicate that extrapolating localized ecological observations to broader engineering impact zones may

introduce spatial uncertainty [24], thus spatial differences in hydrodynamic conditions and water-quality characteristics should be fully considered [25]. This study aims to address the aforementioned challenges by developing an integrated spatial downscaling framework. The framework quantifies dredging-associated ecological losses at a refined spatial resolution. Sparse ecological monitoring data were transformed into a high-resolution spatial continuum.

This study aims to address the spatial-scale mismatch between sparse ecological monitoring data and fine-scale engineering-induced disturbances in estuarine dredging areas. Firstly, sparse aquatic ecological monitoring data are often insufficient to directly support engineering loss assessment because discrete sampling stations have limited spatial coverage. Secondly, direct extrapolation from monitoring stations may introduce large uncertainty when ecological responses vary across heterogeneous eco-hydrodynamic zones. Thirdly, the ecological biomass losses and associated economic losses under dredging and silt-curtain mitigation scenarios were estimated in this study. Specifically, a three-tiered modeling approach was introduced. First, the irregular estuarine domain was partitioned into distinct zones to capture the spatial heterogeneity of the river-to-sea transition. Second, localized models were established within each zone to evaluate the relationships between environmental factors and biological responses across various aquatic populations. Finally, these models were applied across the entire study area to quantify biomass and economic losses under different mitigation scenarios. By linking hydrological simulation outputs with biological observations, the study provides a spatially basis for ecological impact assessment and compensation estimation in data-limited coastal and estuarine regions.

2. Research Methodology

2.1. Study Area and Monitoring Station Layout

The study area is located in the Maowei Sea estuary (an estuary in the northern part of Qinzhou Bay), Guangxi, China as illustrated in Figure 1, where is a tidal estuary at the river-sea interface. The study area was presented in WGS 1984 geographic coordinates to show its location. The result maps were displayed in the WGS 1984 UTM projected coordinate system to better represent distance-related spatial patterns in the model outputs. The region experiences a typical subtropical marine monsoon climate, characterized by abundant sunlight, sufficient heat, and significant seasonal variations in rainfall. The annual mean air temperature is approximately 22.1 °C, and the average annual precipitation reaches around 2170 mm [26]. This specific climatic condition, combined with the continuous freshwater influx, creates a highly dynamic estuarine transition zone. The water environment and hydrodynamic characteristics of the Maowei Sea are strongly influenced by its semidiurnal tidal patterns and riverine discharges.

A waterway dredging project is planned in this estuary that may potentially affect water depth and flow velocity. Within the study area, 29 water environment and aquatic ecology monitoring stations were observed. These stations are evenly distributed across the estuary, covering both nearshore and offshore areas.

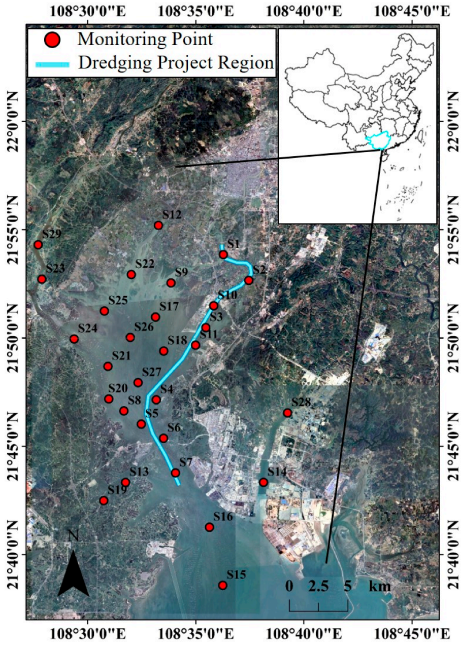


Figure 1. Study Area.

2.2. Integrated SVM-GAM Framework for Ecological Impact Assessment

An integrated framework was developed to analyze the spatial correlations among hydrodynamics, suspended sediment, and ecological variables under dredging scenarios, emphasizing fine-scale statistical evaluations. As shown in Figure 2, the proposed framework assesses estuarine ecological influences through SVM-based spatial zoning for heterogeneity, GAM statistical analysis of physical and biological data, and subsequent quantification of biomass and economic losses under mitigation scenarios.

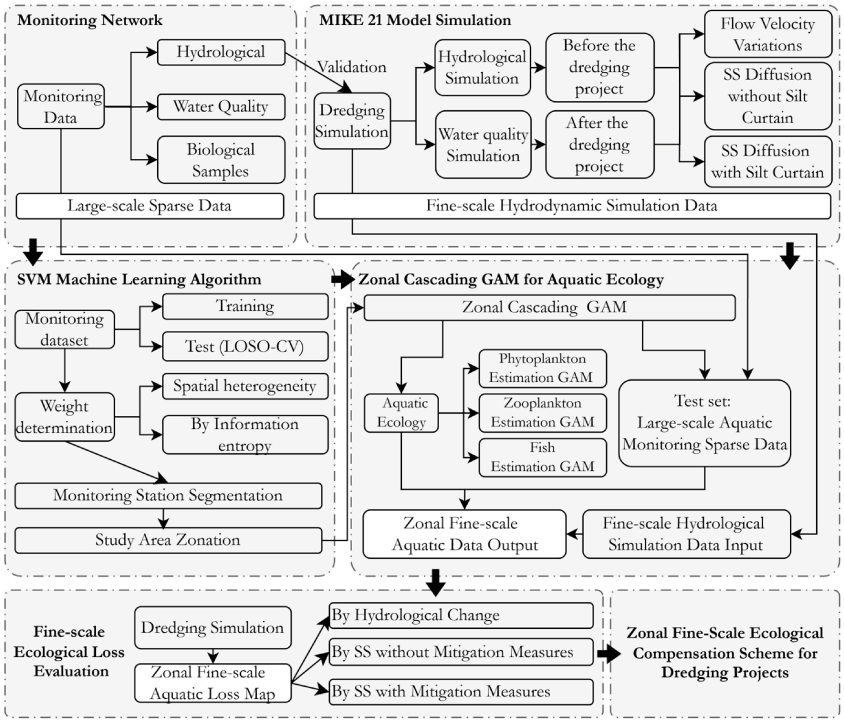


Figure 2. Methodological Framework.

First, scenarios of conventional dredging and dredging with silt curtains were used in a hydrodynamic and water-quality model to predict the changes in current fields and sediment distribution brought about by dredging. Second, the study used an entropy-weighted SVM to divide the estuarine–coastal water body into discrete eco-hydrodynamic zones to address limited monitoring coverage. By capturing the regional variability of the water body, this division produced a framework for downscaling ecological variables. Third, a chained GAM was constructed to statistically relate hydrodynamic factors, primary producers, secondary consumers, and fish biomass across the defined zones. Finally, the study integrated sediment exposure data with literature-based loss rates for different trophic levels to estimate ecological damage.

2.3. Hydrodynamic and Water Environment Influence Modeling

A high-resolution hydrodynamic model was developed utilizing the MIKE software 2014 to assess the environmental and hydrodynamic changes caused by these activities. The finite volume approach was used to discretize the model equations. The computational domain was represented by an unstructured triangular mesh to accurately capture complex coastal geometry. The mesh was refined to 65,023 elements, providing a spatial resolution of approximately 20 m in key areas. Boundary conditions were specified using synchronized tidal and meteorological observational data. Validation against field-measured water levels and current velocities confirmed that the model accurately captures the regional tidal constituents (as illustrated in Supplementary Figure S1). Simulated trends generally align with monitoring records, yielding Nash-Sutcliffe Efficiency (NSE) values ranging from 0.636 to 0.923.

The transport and fate of suspended solids during dredging were quantified using a two-dimensional, unsteady-state advection-diffusion model integrated within a water-quality framework. In this simulation, dredging operations were parameterized as dynamic point sources. The model assessed sediment dispersion under both unmitigated scenarios and mitigated conditions involving the deployment of silt curtains. For ecological risk assessment, the excess suspended sediment concentrations were classified into five discrete intervals: 10–20, 20–50, 50–100, 100–150, and >150 mg/L.

Simulations were conducted using the MIKE21 suite to compare the baseline hydrodynamic regime with post-dredging conditions. These outputs served as the physical forcing functions for subsequent models.

2.4. Spatial Partitioning via Entropy-Weighted SVM

This study divided the estuarine-coastal water body into discrete eco-hydrodynamic zones using an entropy-weighted SVM framework. This method specifically addresses the intrinsic spatial non-stationarity and heterogeneity of the river-to-sea transition [27]. By integrating entropy weights that prioritize environmental factors with greater information gain, the model improves classification of longitudinal gradients and localized transition patches. This approach is novel because it can distinguish nonlinear boundaries between river-dominated and marine-dominated conditions, providing a spatially explicit foundation for subsequent ecological modeling.

Environmental and biological data from 29 monitoring sites were compiled and supplemented with high-resolution downscaling points. The dataset included physicochemical variables such as pH, dissolved oxygen, and chemical oxygen demand. It also included biological indicators such as chlorophyll-a concentration and the numbers of species groups for algae, fish, and benthos (as listed in Supplementary Table S1). The classification procedure grouped these data into distinct eco-hydrodynamic classes, providing a spatially explicit representation of the estuary's dynamic disturbance zones.

The SVM serves as the primary tool for spatial classification by identifying an optimal hyperplane that maximizes the margin between different environmental clusters in a high-dimensional feature space. The decision function for the classification is defined as follows:

$$f(x) = \text{sgn}(\sum_{i=1}^{n} y_i \alpha_i K(x, x_i) + b) \quad (1)$$

In this formulation:

$f(x)$ represents the predicted eco-hydrodynamic class for a given spatial point;

y_i denotes the class labels of the training data points;

α_i are the Lagrange multipliers determined during the optimization process;

$K(x, x_i)$ is the kernel function, which maps the input variables into a higher-dimensional space to handle nonlinear ecological boundaries;

b is the bias term of the optimal hyperplane.

The entropy weight w_j is incorporated into the input vector x to scale the influence of each physicochemical or biological parameter based on its contribution to the system's total information entropy. The entropy weights were calculated from the monitoring data. This gives greater influence to variables exhibiting significant gradients.

2.5. Chained Ecological GAM Framework

The chained GAM framework was used to examine nonlinear statistical associations among modeled hydrodynamic variables, phytoplankton, zooplankton, and fish abundance. By decomposing global ecological relationships into localized environmental units based on data from 29 monitoring stations, the model captures spatial non-stationarity.

GAM was used to establish the relationship between fish abundance and ecological covariates, facilitating the representation of nonlinear effects through smooth functions of explanatory variables. The model assumes the expected value of the response variable is related to a sum of smooth basis functions of the predictors:

$$E(Y) = \beta_0 + \sum_{i=1}^{p} f_i(X_i) \quad (2)$$

where:

$E(Y)$ is the expected fish abundance;

β_0 is the model intercept;

X_i represents the explanatory variables of flow velocity, phytoplankton density, and zooplankton density;

f_i denotes the smooth functions constructed from linear combinations of basis functions.

In the localized models, these functions are operationalized through specific basis terms $B[s0]$ and $B[s1]$. This allows the capture of complex, non-monotonic curves. The coefficients of these basis functions determine the direction and magnitude of effects within each spatial unit, identifying nonlinear parabolic, threshold, or inhibitory responses.

Data from 29 monitoring stations served as ecological calibration and validation points for establishing statistical relationships between biological variables and high-resolution hydrodynamic and water-quality factors. These stations covered the main eco-hydrodynamic zones identified by the entropy-weighted SVM classification, including riverine, transitional, and marine-dominated areas. To maintain fitting accuracy while preventing overfitting, a penalty term was integrated into the estimation process to discourage excessive complexity in the basic functions. Furthermore, maintaining a consistent set of explanatory variables across all clusters improved the reliability of model fitting.

2.6. Performance Evaluation of the SVM-Zonal Chained GAM Framework

To evaluate the proposed SVM-zonal chained GAM, its predictive performance was compared with five benchmark methods, including the mean baseline, inverse distance weighting (IDW), global linear model, global GAM, and random forest [28,29]. Model accuracy was assessed using RMSE and R^2, and residual Moran's I was used to examine the remaining spatial autocorrelation. The results are presented in Table 1 which reports validation metrics for fish abundance.

Table 1. Comparison of predictive performance among methods.

Method	RMSE	R^2	Moran's I
Mean baseline	0.142	−0.039	0.014
Inverse distance weighting, IDW	0.138	0.023	−0.038
Global linear model	0.096	0.526	−0.049
Global GAM	0.095	0.537	−0.058
Random forest	0.095	0.536	−0.082
SVM-zonal chained GAM	0.051~0.103	0.604~0.882	−0.305~−0.047

The SVM-zonal chained GAM showed better predictive performance. It achieved a lower simulation RMSE, ranging from 0.051 to 0.103, and clearly outperformed other methods in explanatory power, with R^2 increasing to 0.604~0.882 compared with 0.537 for the global GAM and 0.536 for random forest. Residual Moran's I of SVM-zonal chained GAM ranged from −0.305 to −0.047, indicating that the method better captures spatial heterogeneity and reduces residual spatial clustering compared with the global models.

The proposed SVM-zonal chained GAM framework is applicable to data-limited estuarine projects. It is particularly useful for capturing spatial non-stationarity and supporting ecological loss and compensation assessment. However, its transferability depends on the representativeness of monitoring stations and the accuracy of physical model outputs. Therefore, it should be applied with uncertainty analysis and, where possible, independent spatial validation.

2.7. Assessment of Marine Ecological Losses Correlate with Dredging

This study estimated the loss of phytoplankton, zooplankton, and fish resources associated with SS dispersion during estuarine dredging project using a quantitative impact-assessment approach.

Biological resource densities D_{ij} were derived from regional downscaling calculations. The spatial extent of the influence zones S_{ij} and SS concentration increments were simulated based on dredging activity parameters. The design dredging depth was established at 5 m, taking into account the navigation channel grade and prevailing bathymetric conditions. To determine the loss rates K_{ij}, we synthesized empirical data from existing literature, categorized by varying SS concentration ranges.

The primary calculation for the total loss of biological resource i W_i is defined by the following summation [30]:

$$W_i = \sum_{j=1}^{n} D_{ij} \times S_{ij} \times K_{ij} \quad (3)$$

where:

W_i represents the one-time average loss of resource type i (measured in individuals, units, or kg);

D_{ij} is the density of resource i within the j^{th} concentration increment zone;

S_{ij} denotes the area of the j^{th} concentration increment zone;

K_{ij} is the corresponding loss rate;

n is the total number of defined concentration increment zones.

In accordance with regulatory standards [30], the economic compensation for these resources is set at three times the calculated physical loss. The total economic loss M_i for resource i is subsequently calculated as:

$$M_i = W_i \times E_i \quad (4)$$

where E_i represents the commodity price of the resource (Yuan/kg), determined by the average local market wholesale price over the preceding three years.

3. Results

3.1. Hydrodynamic and Water Quality Modeling of Dredging Operations

3.1.1. Flow Velocity and Current Pattern Changes

Hydrodynamic modeling (as illustrated in Figure 3) reveals that while the dredging project will cause a minor 4.24% reduction in the overall average flow velocity (from 0.172 to 0.165 m/s), localized velocities within the waterway increased, ranging from 0.95 to 1.80 m/s. During flood tides, flow velocities along the navigation channel increased by up to 1.0 m/s, with the most significant acceleration observed at the river-ocean strait and exacerbated by upstream discharge. Conversely, influences outside the channel were minimal, exhibiting negligible changes (0.2 to 0.2 m/s) in adjacent areas and the outer sea. Overall, the project altered the local tidal-current field, but large-scale hydrodynamic influences remained limited.

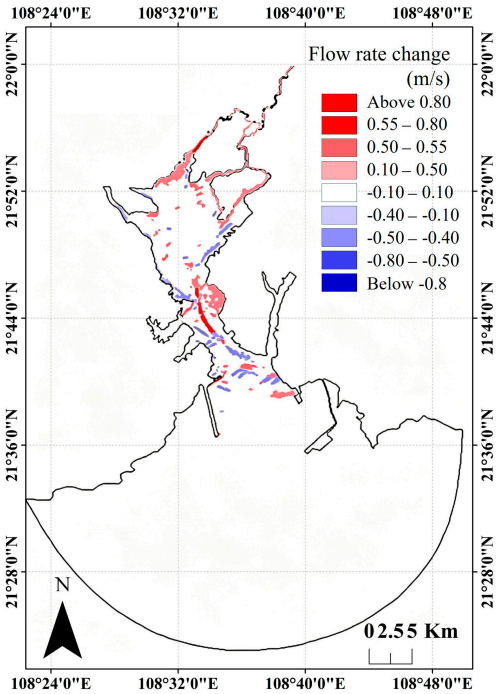


Figure 3. Spatial distribution of maximum current velocity changes before and after dredging.

3.1.2. Suspended Sediment Distribution During Dredging

Simulations were conducted for two scenarios as illustrated in Figure 4: conventional dredging without protective measures and dredging with silt curtains deployed. Without protective measures, the area affected by suspended sediment concentrations exceeding 10 milligrams per liter reached 22.5 km^2. Areas with concentrations between 20 and 50 milligrams per liter covered 26.2 km^2. Regions experiencing concentrations between 50 and 100 milligrams per liter spanned 11.36 km^2. The most severely influenced areas, with concentrations exceeding 150 milligrams per liter, encompassed 21.2 km^2.

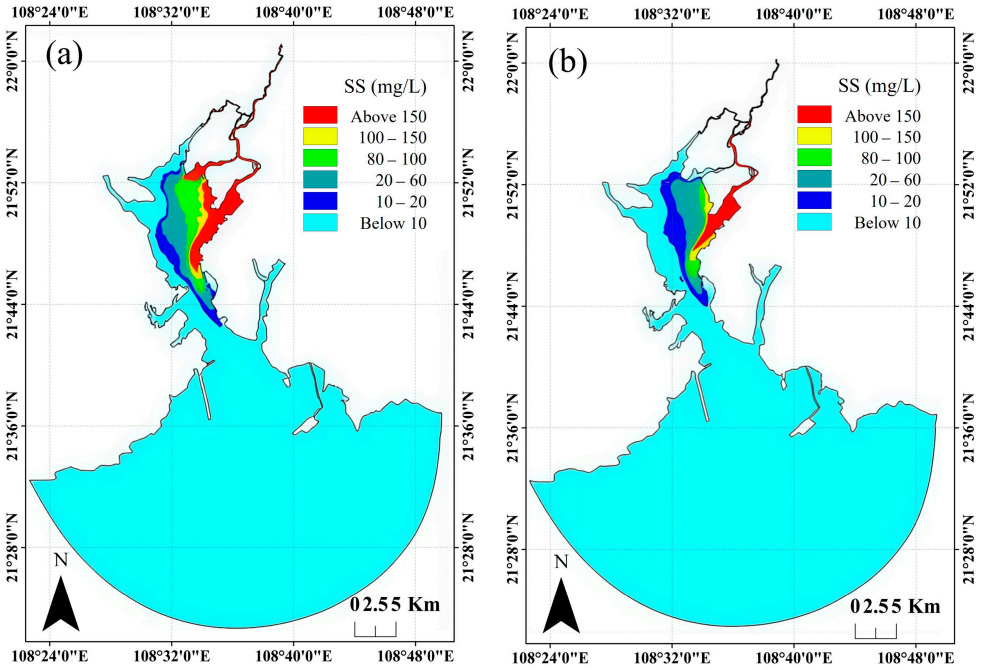


Figure 4. Simulation maps of the SS influence range during dredging. (**a**) SS Increment without silt curtains. (**b**) SS Increment with silt curtains.

Implementation of silt curtains substantially reduced the spatial extent of suspended sediment influences. As listed in Table 2, the area affected by concentrations between 10 and 20 milligrams per liter decreased to 21.1 km^2, representing a 6.2% reduction. More pronounced reductions occurred in higher concentration zones. Areas experiencing 20 to 50 milligrams per liter decreased by 39.7% to 15.8 km^2. Regions with 50 to 100 milligrams per liter showed a 41.5% reduction to 6.64 km^2. The most dramatic improvement occurred in the 100 to 150 milligrams per liter range, which decreased by 71.8% to 2.2 km^2. Areas exceeding 150 milligrams per liter were reduced by 38.2% to 13.1 km^2. These results demonstrated that silt curtain deployment provided effective mitigation of suspended sediment dispersion, particularly in zones experiencing the highest concentration levels.

Table 2. Comparison of dredging-associated influence areas under scenarios with and without silt curtains.

Concentration Range (mg/L)	Without Silt Curtains Area (km^2)	With Silt Curtains Area (km^2)	Reduction Rate (%)
10~20	22.5	21.1	6.2
20~50	26.2	15.8	39.7
50~100	11.36	6.64	41.5
100~150	7.8	2.2	71.8
>150	21.2	13.1	38.2

3.2. Eco-Hydrodynamic Zoning Using Entropy-Weighted SVM

The entropy-weighted SVM partitioned the irregular estuarine–coastal water body into five distinct eco-hydrodynamic zones (Classes 1–5).

This classification captured clear spatial differences that are typical of the river-to-sea transition. The resulting spatial distribution (Figure 5) shows a longitudinal gradient from river-dominated to marine-dominated conditions. It also shows localized transition patches that reflect complex mixing and hydrological patterns.

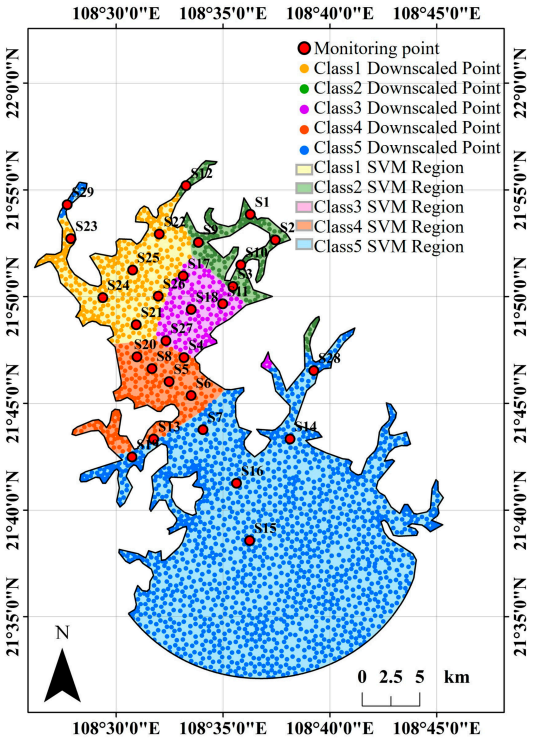


Figure 5. Classification of monitoring sites and simulated hydrodynamic data within the five SVM-based eco-hydrodynamic partitions.

As listed in Table 3, Class 5 dominated the downscaling domain at 66.6% despite containing only 24.14% of the monitoring sites. In contrast, Classes 2–4 represented substantial portions of the monitoring network but accounted for relatively small fractions of the total downscaling points. Classes 2–4 are areas where riverine and marine influences alternate along the river-to-sea gradient. In contrast, Class 5 is mostly marine-dominated, so it was not fragmented into smaller, disconnected patches. This difference indicates that the fine-resolution reconstruction was primarily concentrated in the alternating river–sea disturbance zone.

Table 3. Distribution of monitoring sites and downscaling points across the five identified classes.

Class	Monitoring Points (%)	Downscaling Points (%)
Class1	20.69%	12.50%
Class2	20.69%	6.74%
Class3	13.80%	5.70%
Class4	20.69%	8.47%
Class5	24.14%	66.60%

Physicochemical variables varied among the identified classes. pH values decreased significantly, from 8.12 in Class 1 to 7.65 in Class 5. Additionally, dissolved oxygen declined along the class gradient, beginning at 8.13 mg/L in Class 1 and reaching 7.34 mg/L in Class 5. These results are consistent with the general pattern that inland flowing waters usually have higher DO concentrations than marine-influenced coastal waters.

A localized deterioration of water quality was observed in Class 2, where concentrations of chemical oxygen demand, nitrates, and total suspended solids reached their respective peaks. This zone primarily represents inland riverine segments characterized by restricted water exchange capacity, which likely facilitates the accumulation of these pollutants.

Biological indicators showed clear changes in community structure along the estuarine gradient. Chlorophyll-a levels were higher in Classes 1–3, averaging about 11.5 μg/L, but much lower in Classes 4–5. This suggests that the upper reaches and river-dominated transition zones provide more favorable conditions for phytoplankton growth. Phytoplankton density remained high in Classes 1–2 with a mean of 0.69, which was consistent with this pattern. Fish abundance, by contrast, increased downstream and reached its highest value in Class 5 at 0.11. This pattern indicates that marine-dominated areas may support more complex food webs. In contrast, benthic richness showed no clear regional difference and was distributed relatively evenly across the study area.

3.3. Zonal GAM-Based Predicted Biomass Responses

Drawing on data from 29 monitoring stations, we established a chained GAM framework integrating hydrodynamics, primary producers, secondary consumers, and fish. Supported by SVM-based spatial partitioning, distinct GAM response models for fish were constructed across five environmental units as illustrated in Figure 6. Specifically, hydrodynamics was used to explain water-quality variation; hydrodynamics and water quality were then used to explain phytoplankton; hydrodynamics, water quality, and phytoplankton were used to explain zooplankton; and hydrodynamics, water quality, phytoplankton, and zooplankton were used to explain fish distribution. As listed in Table 4, the SVM-zonal chained GAM achieved LOSO-CV RMSE values of 0.054–0.097 and MAE values of 0.042–0.067 across the five zones, indicating that the average prediction error was approximately 0.04–0.10 index units. The predictive LOSO-CV R^2 ranged from 0.609 to 0.865, showing that all zonal models explained more than 60% of the variation at withheld stations. Spatial uncertainty was evaluated using cross-validation residuals. The LOSO-CV residual Moran's I ranged from −0.238 to −0.119, suggesting that no positive residual spatial autocorrelation remained and that the framework effectively captured spatial heterogeneity.

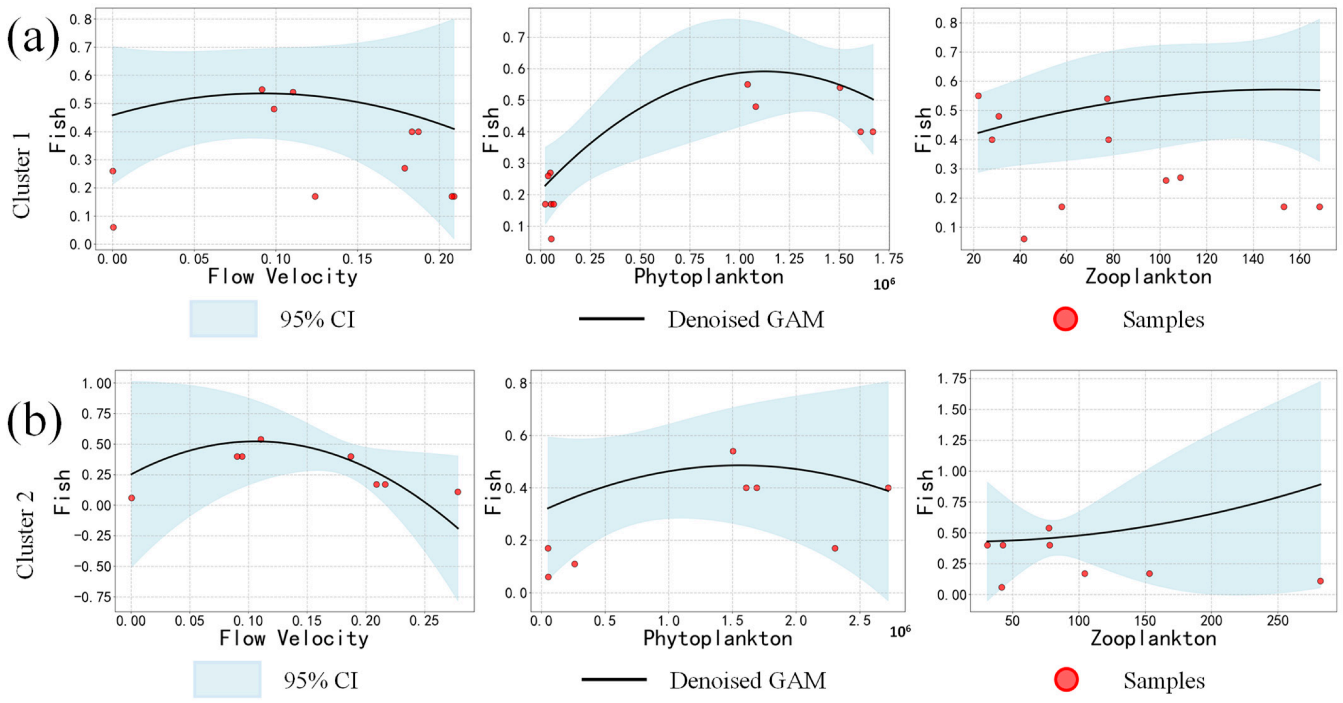


Figure 6. *Cont.*

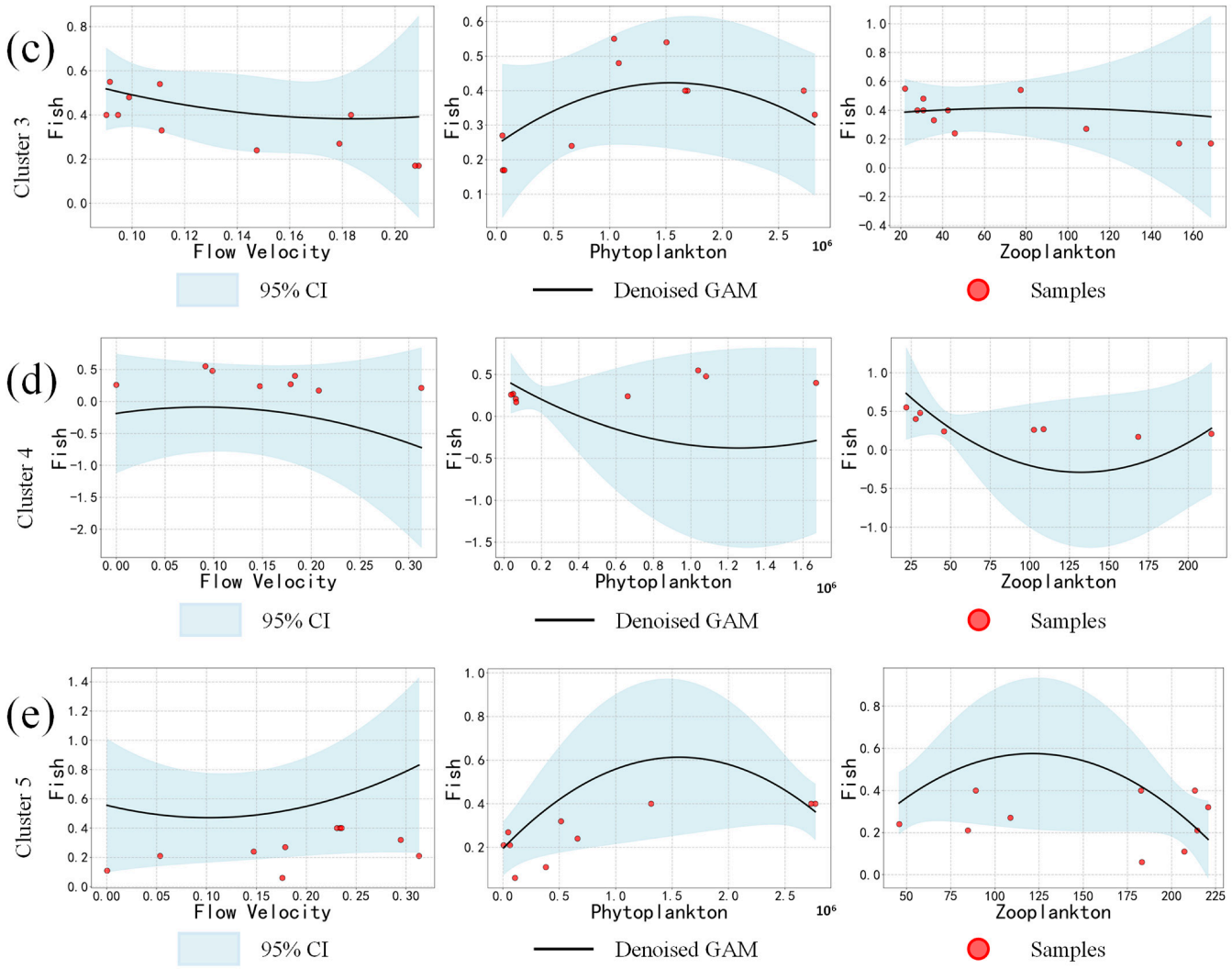


Figure 6. GAM-based response curves of fish to hydrodynamic stressors and aquatic organism availability. (**a**) Cluster 1: Fish = 0.0605 + (0.1766)·B[s0](Flow Velocity) + (−0.0486)·B[s1](Flow Velocity) + (0.5410)·B[s0](Phytoplankton) + (0.2736)·B[s1](Phytoplankton) + (0.1682)·B[s0](Zooplankton) + (0.1464)·B[s1](Zooplankton). (**b**) Cluster 2: Fish = 0.0470 + (0.7064)·B[s0](Flow Velocity) + (−0.4430)·B[s1](Flow Velocity) + (0.2902)·B[s0](Phytoplankton) + (0.0659)·B[s1](Phytoplankton) + (0.0312)·B[s0](Zooplankton) + (0.4602)·B[s1](Zooplankton). (**c**) Cluster 3: Fish = 0.3300 + (−0.1705)·B[s0](Flow Velocity) + (−0.1261)·B[s1](Flow Velocity) + (0.3102)·B[s0](Phytoplankton) + (0.0468)·B[s1](Phytoplankton) + (0.0723)·B[s0](Zooplankton) + (−0.0322)·B[s1](Zooplankton). (**d**) Cluster 4: Fish = 1.2192 + (0.3490)·B[s0](Flow Velocity) + (−0.5338)·B[s1](Flow Velocity) + (−1.0337)·B[s0](Phytoplankton) + (−0.6837)·B[s1](Phytoplankton) + (−1.7831)·B[s0](Zooplankton) + (−0.4521)·B[s1](Zooplankton). (**e**) Cluster 5: Fish = 0.0361 + (−0.2582)·B[s0](Flow Velocity) + (0.2748)·B[s1](Flow Velocity) + (0.7381)·B[s0](Phytoplankton) + (0.1662)·B[s1](Phytoplankton) + (0.5448)·B[s0](Zooplankton) + (−0.1723)·B[s1](Zooplankton).

Table 4. Statistical performance of the SVM-zonal chained GAM in five zones.

Cluster	Stage	R^2	RMSE	MAE	Moran's I
Cluster 1	Sample Simulation	0.882	0.0562	0.0456	−0.0471
	LOSO-CV Verification	0.865	0.06	0.0424	−0.19
Cluster 2	Sample Simulation	0.604	0.103	0.068	−0.305
	LOSO-CV Verification	0.609	0.0968	0.0671	−0.238
Cluster 3	Sample Simulation	0.844	0.0509	0.0414	−0.124
	LOSO-CV Verification	0.827	0.0538	0.047	−0.225
Cluster 4	Sample Simulation	0.805	0.0645	0.0493	−0.0731
	LOSO-CV Verification	0.797	0.065	0.0467	−0.12
Cluster 5	Sample Simulation	0.747	0.0598	0.055	−0.275
	LOSO-CV Verification	0.725	0.0599	0.043	−0.184

Moreover, the results underscore considerable spatial non-stationarity in fish responses, as identical factors demonstrated diverse effect directions and combinations across distinct spatial units, a complexity that a single global model cannot capture. Distinct response patterns of fish to hydrodynamic conditions were observed across clusters. In Cluster 1, Cluster 2, and Cluster 4, the flow velocity terms showed a combination of positive and negative basis function coefficients, such as +0.1766 and −0.0486 in Cluster 1, and +0.7064 and −0.4430 in Cluster 2. This reflects a typical nonlinear structure where flow velocity does not exert a monotonic effect on fish but instead suggests the presence of threshold or optimal range characteristics. Conversely, both flow velocity coefficients in Cluster 3 were negative at −0.1705 and −0.1261, indicating that fish in this unit show a negative statistical association with increased hydrodynamic forcing. Cluster 5 presented a negative-positive combination of −0.2582 and +0.2748, showing a nonlinear form distinct from other clusters and further supporting the existence of differentiated hydrodynamic-habitat suitability relationships across different environmental zones. Spatial divergence in response to trophic factors was even more pronounced.

The cluster-specific coefficients showed clear heterogeneity in the relationships associated with phytoplankton and zooplankton. Positive coefficients were observed in Cluster 5, with values of +0.7381 and +0.5448, respectively. Cluster 1 also showed positive coefficients, although the magnitude was lower, particularly for zooplankton, with values of +0.5410 for phytoplankton and +0.1682 for zooplankton. In contrast, Cluster 4 exhibited negative coefficients for both biological variables. The phytoplankton-related coefficients in Cluster 4 were −1.0337 and −0.6837, while the zooplankton-related coefficients were −1.7831 and −0.4521. These negative values indicate that Cluster 4 differed from the other clusters not only in coefficient direction but also in coefficient magnitude, especially for zooplankton, where the absolute value of −1.7831 was larger than the corresponding values reported for the other clusters.

3.4. Quantification of Cascading Ecological Influences Under Dredging-Associated Stressors

3.4.1. Assessment of Model-Estimated Ecological Changes Associated with Hydrodynamic Alterations Following Dredging Activities

Biological resource density data for phytoplankton, zooplankton, and fish were derived from the spring 2021 and autumn 2021 surveys conducted by Guangxi Liuhuan Environmental Protection Co., Ltd. and the Guangxi Zhuang Autonomous Region Marine Geological Survey Institute in the waters adjacent to the project. The spring 2021 and autumn 2021 surveys did not collect fish egg and larval samples, so the resource density calculations used fish egg survey data in Maowei Sea April 2021. Influence water-depth calculations assumed an average water depth of approximately 5 m in the project area.

The hydrodynamic simulation indicated local changes in flow velocity under the dredging scenario. The chained GAM then projected spatially heterogeneous biological changes that were statistically associated with these hydrodynamic covariates, as illustrated in Figure 7. In the northern upstream sectors and narrow channel segments, flow velocity showed a widespread decreasing trend with local reductions ranging from 20.0% to 38.1%. Conversely, the transition zones and open waters near the southern offshore area exhibited an increasing trend in flow velocity, with peak increments exceeding 4.0% in the southern core area. This spatial pattern indicates that dredging improved water-exchange efficiency in the southern region.

The modeled spatial distribution of plankton was highly consistent with changes in flow velocity and showed a significant positive correlation with flow-velocity changes. In the northern riverine section, influenced by the reduction in flow velocity, phytoplankton biomass showed a general decline, with reductions ranging from 5.0% to 23.42%. Meanwhile, the southern offshore areas and central shoals showed significant growth, with increments concentrated between 1.0% and 4.0%. The response range of zooplankton to the waterway dredging project largely overlaps with that of phytoplankton. Affected by the weakened upstream discharge, the change rate of zooplankton in the northern region was negative, whereas multiple growth hotspots emerged in the southern offshore end with maximum change rates exceeding 4.0%. This observation suggests that the increase in flow velocity was associated with dredging may promote vertical mixing of nutrients or accelerate the influx of high-nutrient water masses from the open sea, thereby driving the overall increase in plankton biomass.

Compared with primary and secondary productivity, changes in fish biomass were relatively moderate in magnitude and showed greater spatial diffusion. Fish biomass in the northern channel area showed a slight decrease, with most reductions remaining within 2.0%. In the southern offshore region, fish showed a low-intensity growth trend of approximately 1.0% to 3.0%. Notably, the high-growth zones for fish were less concentrated than those for flow velocity but instead show a broad and uniform distribution. These analytical results indicate that higher-trophic-level organisms were less sensitive to physical habitat alterations than plankton. For organisms at higher trophic levels, the direct physical effects associated with dredging activities may be attenuated.

Integrating the four assessment indicators, the ecological response following dredging displayed clear north–south polarization. The northern upstream channel region is characterized by physical deceleration and biomass decline, where the alteration of the physical environment is most intense. In contrast, the southern offshore region is characterized by hydrodynamic enhancement and an overall increase in biomass, reflecting the potential contribution of dredging to coastal resource compensation.

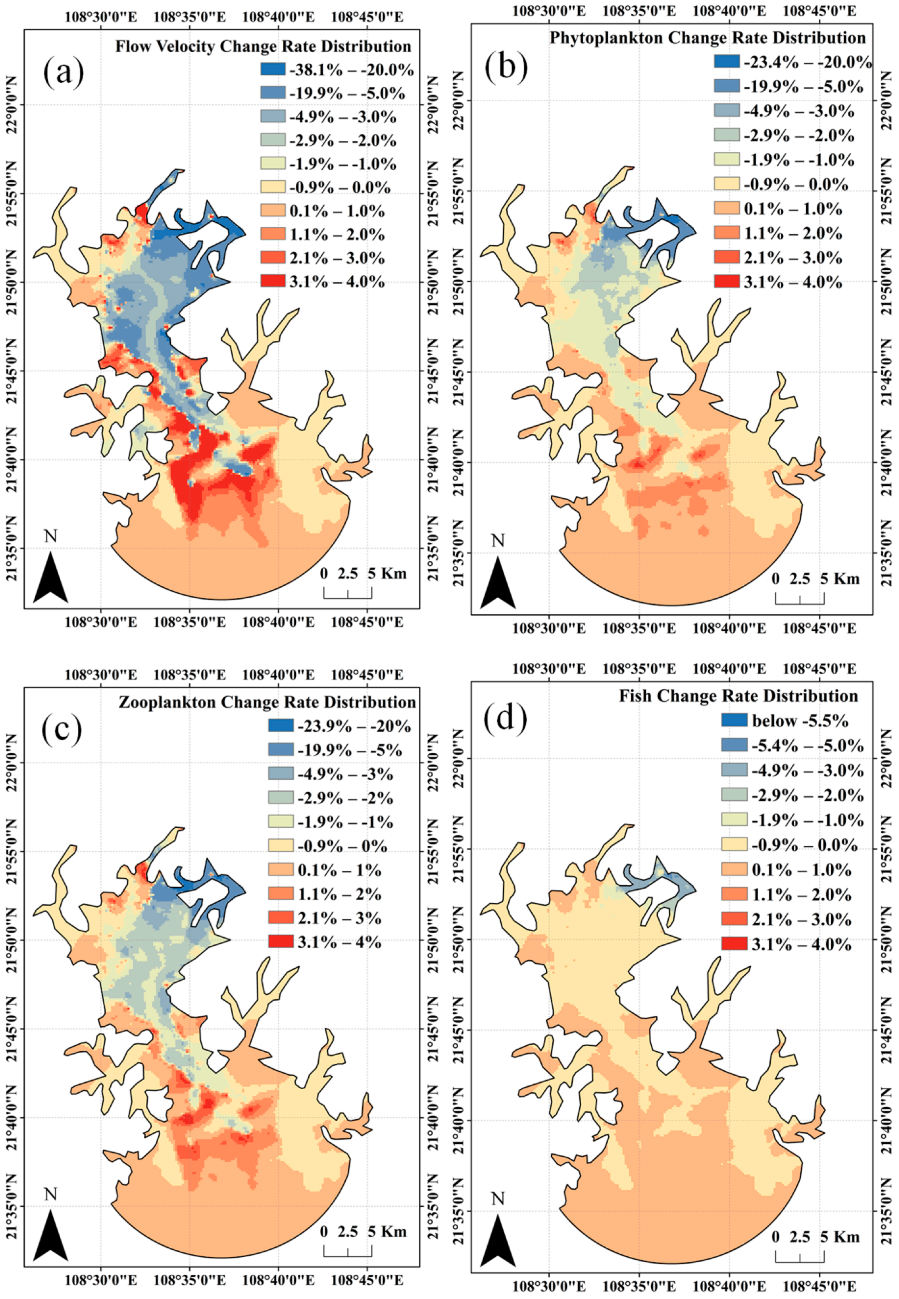


Figure 7. Spatial distribution of simulated hydrodynamic changes and model-estimated ecological changes under the dredging scenario. (**a**) Flow velocity change rate distribution. (**b**) Phytoplankton change rate distribution. (**c**) Zooplankton change rate distribution. (**d**) Fish change rate distribution.

3.4.2. Assessment of Estimated Ecological Losses Under Dredging-Derived Suspended-Sediment Exposure

The dispersion of suspended sediment was associated with dredging activities was simulated based on the previously modeled variations in the hydrodynamic field. The loss rate coefficients for fish [31–33], zooplankton [34–36], and phytoplankton [34,37,38] across defined suspended sediment (SS) gradients were established through a synthesis of established ecological literature, as listed in Table 5.

Table 5. Dredging-period loss-rate estimates for fish, zooplankton, and phytoplankton.

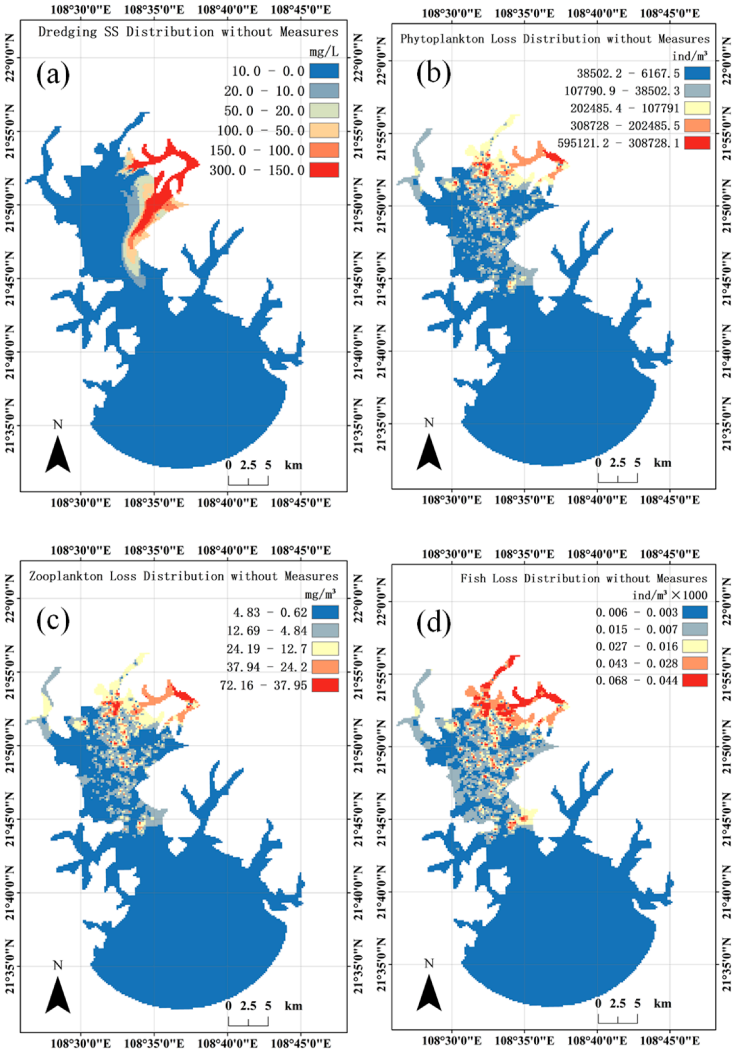
Suspended Sediment Range	Resource Type	Loss Rate
>150 mg/L	Fish	15–25%
	Zooplankton	50–70%
	Phytoplankton	60–80%
100–150 mg/L	Fish	10–15%
	Zooplankton	40–55%
	Phytoplankton	40–55%
50–100 mg/L	Fish	5–10%
	Zooplankton	25–40%
	Phytoplankton	25–40%
20–50 mg/L	Fish	1–5%
	Zooplankton	10–20%
	Phytoplankton	10–20%
10–20 mg/L	Fish	0–1%
	Zooplankton	2–8%
	Phytoplankton	2–8%
0–10 mg/L	Fish	0–1%
	Zooplankton	0–2%
	Phytoplankton	0–2%

The dispersion of suspended sediment (SS) generated by dredging activities exerted a substantial influence on the multi-trophic biomass within the study area, whereas the deployment of silt curtains provided measurable mitigation of this ecological disturbance. According to the biological loss estimates (with 95% confidence intervals listed in Table 6), the estimated losses of phytoplankton and zooplankton in the absence of mitigation measures reached 6.0×10^{12} ind and 7.7×10^{8} mg, respectively. By implementing silt curtains as a core mitigation strategy, the losses for these two lower trophic categories were reduced to 5.3×10^{12} ind and 7.0×10^{8} mg, corresponding to reductions of 11.4% and 9.6%, respectively. This protective efficacy was particularly pronounced in the high-influence core zones where SS concentrations exceeded 150 mg/L, as the loss rates for phytoplankton and zooplankton in these specific concentration intervals were as high as 60.0% to 80.0% and 50.0% to 70.0%, respectively.

Table 6. Quantification of biomass losses associated with dredging-derived suspended sediment exposure.

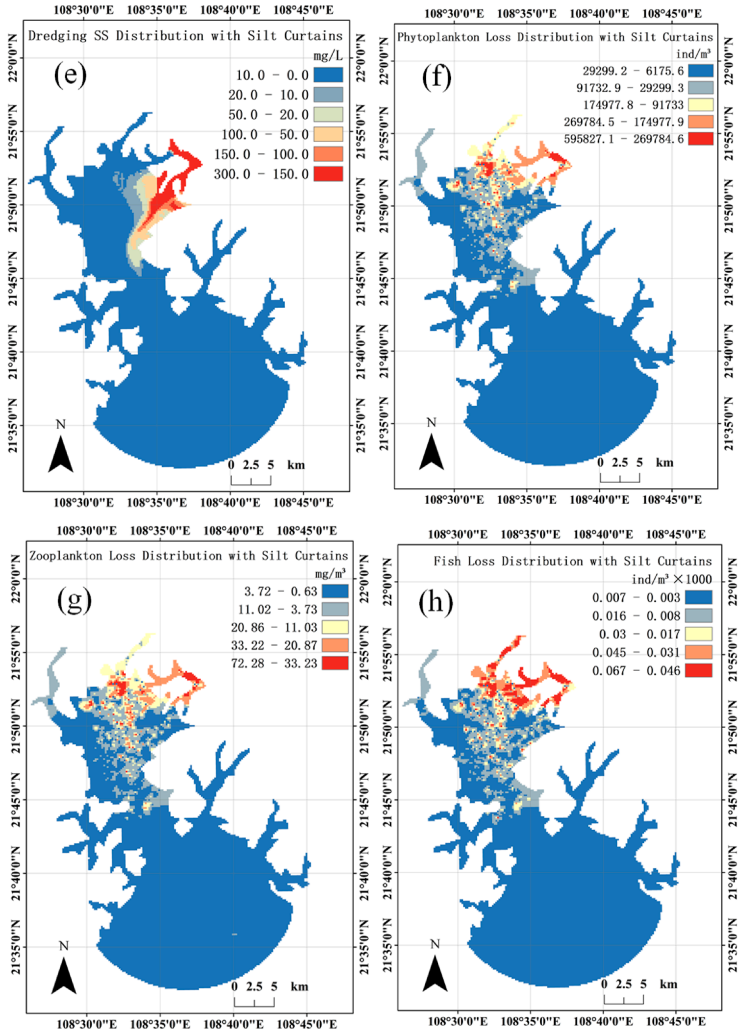
	Without Mitigation Measures		With Silt Curtains		Reduction Rate (%)
	Amount	Price (Million CNY)	Amount	Price (Million CNY)	
Phytoplankton Loss (ind)	6.00×10^{12} (5.33×10^{12}~6.67×10^{12})	0.017 (0.015~0.019)	5.30×10^{12} (4.66×10^{12}~5.94×10^{12})	0.015 (0.013~0.017)	11.4 (10.9~12.6)
Zooplankton Loss (mg)	7.70×10^{8} (6.77×10^{8}~8.63×10^{8})	2.50 (2.20~2.80)	7.00×10^{8} (6.08×10^{8}~7.92×10^{8})	2.20 (1.91~2.49)	9.6 (8.2~10.2)
Fish Loss (kg)	1.25×10^{6} (1.01×10^{6}~1.49×10^{6})	24.02 (19.47~28.58)	1.20×10^{6} (9.57×10^{5}~1.44×10^{6})	23.13 (18.73~27.53)	4.0 (3.4~5.2)
Total (million CNY)	26.54 (21.97~31.12)		25.34 (20.65~30.04)		4.5 (3.5~6.0)

Spatial distribution results further indicate that physical barriers provided different levels of protection across ecological tiers (as illustrated in Figure 8). Variations in plankton loss exhibited a high degree of spatial coupling with the localized reduction in SS concentrations. By intercepting sediment particles, silt curtains significantly reduced the spatial coverage where SS increments exceeded 100.0 mg/L, thereby directly decreasing the biological population exposed to high-concentration environments. In contrast, the reduction in fish loss is notably lower at only 4.0%, with the total biomass loss slightly adjusting from 1.25×10^6 kg to 1.20×10^6 kg. Such a relatively moderate response mechanism suggests that fish, as higher-trophic-level organisms, have greater capacity for active migration, rendering them less sensitive to localized physical habitat improvements compared to passively drifting plankton.



(1)

Figure 8. *Cont.*



(**2**)

Figure 8. (**1**) Distribution of Dredging-Derived SS without Mitigation Measures. (**2**) Distribution of Dredging-Derived SS with Silt Curtains. (**a**) SS Increment without silt curtains. (**b**) Phytoplankton Loss without silt curtains. (**c**) Zooplankton Loss without silt curtains. (**d**) Fish Loss without silt curtains. (**e**) SS Increment with silt curtains. (**f**) Phytoplankton Loss with silt curtains. (**g**) Zooplankton Loss with silt curtains. (**h**) Fish Loss with silt curtains.

Using three-year compensation calculations and biological resource prices from the Comprehensive Value Price Calculation Table for Guangxi Fishery Resources (2019–2024), compiled by the Guangxi Aquatic Animal Husbandry and Veterinary Bureau, zooplankton losses were converted to fishery resources using the trophic-level one-tenth conversion law. Fish eggs were calculated at 1% survival to commercial fry specifications, and fish larvae at 5% survival to commercial fry specifications. From an ecological value perspective, the implementation of mitigation measures reduced the total economic loss from 26.54 million CNY to 25.34 million CNY, representing an approximately 4.5% reduction in economic loss. Although the high unit price of fish resources caused the proportional change in the total economic loss to remain relatively flat, the 11.4% and 9.6% reductions in losses for primary and secondary productivity demonstrated the critical role of targeted physical barriers in maintaining the structural stability of the underlying ecosystem.

4. Discussion

The present study provides a methodological extension to existing estuarine dredging influence assessments by linking hydrodynamic simulation, spatial zoning, ecological response modeling, and loss quantification within a single workflow. Previous studies have mainly emphasized the effects of dredging-related suspended sediment on water quality and aquatic organisms, including phytoplankton, zooplankton, and fish [3–6]. Numerical models have also been widely used to simulate hydrodynamic and water-quality changes caused by engineering activities. Compared with these studies, the present framework further attempts to translate simulated physical disturbance fields into spatially explicit biological loss estimates under limited monitoring conditions. By using entropy-weighted SVM zoning and zonal GAMs, this study accounts for spatial heterogeneity and nonlinear ecological responses, which are commonly difficult to represent using a single global model.

The framework may support dredging influence assessment, mitigation-scenario comparison, and ecological compensation planning. However, the modeling results depend on the spatial representativeness of the monitoring stations, the accuracy of simulated hydrodynamic and sediment fields, and literature-derived loss-rate coefficients. The analysis does not fully resolve seasonal variability, long-term recovery processes, or unmeasured ecological factors. Future studies should incorporate independent monitoring data, multi-season observations, uncertainty propagation, and post-dredging ecological surveys to further evaluate the robustness and transferability of the proposed framework.

5. Conclusions

This study developed a spatial downscaling framework combining entropy-weighted SVM zoning, chained GAM modeling, and hydrodynamic and water-quality simulations to estimate dredging-related ecological losses in a data-limited estuarine area. Based on 29 monitoring stations and high-resolution MIKE simulation outputs, the estuarine domain was divided into five eco-hydrodynamic zones, and localized biological response models were constructed for phytoplankton, zooplankton, and fish. The zonal GAMs showed in-sample R^2 values ranging from 0.793 to 0.946, indicating that the selected hydrodynamic and trophic variables captured a substantial portion of the observed spatial variability in fish abundance within different environmental units.

The results showed that dredging was associated with spatially heterogeneous hydrodynamic and ecological responses. The average flow velocity decreased from 0.172 m/s to 0.165 m/s, corresponding to a 4.24% reduction, while localized increases and decreases occurred across different channels and offshore areas. Suspended sediment dispersion represented the main quantified ecological pressure. Without mitigation, the affected area exceeded 21.2 km^2 in the >150 mg/L concentration zone. With silt curtains, this area decreased to 13.1 km^2, while the 100–150 mg/L zone decreased from 7.8 km^2 to 2.2 km^2. Correspondingly, phytoplankton loss decreased from 6.0×10^{12} to 5.3×10^{12} individuals, zooplankton loss from 7.7×10^2 to 7.0×10^2 kg, and fish loss from 1.25×10^6 to 1.20×10^6 kg. The estimated total economic loss decreased from 26.54 million CNY to 25.34 million CNY, equivalent to a 4.5% reduction.

Several limitations should be noted, the results depend on the representativeness of monitoring stations, the transferability of fitted ecological relationships, and the literature-based loss coefficients. Future studies should include additional field observations, independent validation, seasonal monitoring, and uncertainty analysis.

https://doi.org/10.3390/land15071196

Supplementary Materials: The following supporting information can be downloaded at: https://www.mdpi.com/article/10.3390/land15071196/s1. Figure S1: Hydrological Model Simulation and Validation. Table S1: Monitoring station locations and water environment and ecological data.

Author Contributions: Z.L.: Writing—original draft, Methodology, Software, Visualization; Z.H.: Funding acquisition, Writing—review & editing, Resources; L.Z.: Software, Resources, Investigation; D.Y.: Visualization, Validation; J.C.: Data curation, Project administration; N.Z.: Project administration, Supervision, Resources; S.L.: Resources, Software, Investigation; C.Z.: Formal analysis, Supervision, Resources; J.L. (Jie Liu): Formal analysis, Supervision; Y.L.: Investigation, Formal analysis, Funding acquisition; J.L. (Jinpeng Lv): Investigation, Formal analysis; Q.L.: Data curation, Investigation; J.H.: Data curation. All authors have read and agreed to the published version of the manuscript.

Funding: This work was supported by National Key R&D Program of China (No: 2023YFC3208800, No: 2023YFC3108300), the Science and technology development project of Transport Planning and Research Institute of Ministry of Transport (092517-905), Guangxi Science and Technology Major Project (AA23023016), Key Scientific and Technological Projects of the Transportation Industry in Guangxi in 2022 (2022-62).

Institutional Review Board Statement: Not applicable.

Informed Consent Statement: Not applicable.

Data Availability Statement: The data presented in this study are available on request from the corresponding author.

Conflicts of Interest: Author Junhui He was employed by the company Pinglu Cannal Group Co., Ltd. The remaining authors declare that the research was conducted in the absence of any commercial or financial relationships that could be construed as a potential conflict of interest.

References

1. Donázar-Aramendía, Í.; Megina, C.; Miró, J.M.; Florido, M.; Sánchez-Moyano, J.E.; García-Asencio, I.; DelValls, T.Á. Environmental effects of maintenance dredging works in a highly modified estuary: A short-term approach. *Ocean. Coast. Manag.* **2024**, *258*, 107394. [CrossRef]
2. Huang, Y.G.; Yang, H.F.; Jia, J.J.; Li, P.; Zhang, W.X.; Wang, Y.P.; Ding, Y.F.; Dai, Z.J.; Shi, B.W.; Yang, S.L. Declines in suspended sediment concentration and their geomorphological and biological impacts in the Yangtze River Estuary and adjacent sea. *Estuar. Coast. Shelf Sci.* **2022**, *265*, 107708. [CrossRef]
3. Todd, V.L.G.; Todd, I.B.; Gardiner, J.C.; Morrin, E.C.N.; MacPherson, N.A.; DiMarzio, N.A.; Thomsen, F. A review of impacts of marine dredging activities on marine mammals. *ICES J. Mar. Sci.* **2015**, *72*, 328–340.
4. Spearman, J. A review of the physical impacts of sediment dispersion from aggregate dredging. *Mar. Pollut. Bull.* **2015**, *94*, 260–277. [CrossRef] [PubMed]
5. Mestdagh, S.; Ysebaert, T.; Moens, T.; Van Colen, C. Dredging-induced turbid plumes affect bio-irrigation and biogeochemistry in sediments inhabited by *Lanice conchilega* (Pallas, 1766). *ICES J. Mar. Sci.* **2020**, *77*, 1219–1226.
6. Pledger, A.G.; Brewin, P.; Mathers, K.L.; Phillips, J.; Wood, P.J.; Yu, D. The effects of water injection dredging on low-salinity estuarine ecosystems: Implications for fish and macroinvertebrate communities. *Ecol. Indic.* **2021**, *122*, 107244. [CrossRef]
7. Murphy, R.R.; Perry, E.; Harcum, J.; Keisman, J. A generalized additive model approach to evaluating water quality: Chesapeake Bay case study. *Environ. Model. Softw.* **2019**, *118*, 1–13. [CrossRef]
8. Gibson, T.I.; Baillie, C.; Collins, R.A.; Wangensteen, O.S.; Corrigan, L.; Ellison, A.; Heddell-Cowie, M.; Westoby, H.; Byatt, B.; Lawson-Handley, L.; et al. Environmental DNA reveals ecologically relevant spatial and temporal variation in fish assemblages between estuaries and seasons. *Ecol. Indic.* **2024**, *165*, 112215. [CrossRef]
9. Fang, Y.; Huang, R.T.; Zhang, Y.Y.; Zhang, J.; Xi, W.N.; Shi, X.Y. Utilizing machine learning models to grasp water quality dynamic changes in lake eutrophication through phytoplankton parameters. *Front. Environ. Sci. Eng.* **2025**, *19*, 14. [CrossRef]
10. Lewis, D.M.; Thompson, K.A.; MacDonald, T.C.; Cook, G.S. Understanding shifts in estuarine fish communities following disturbances using an ensemble modeling framework. *Ecol. Indic.* **2021**, *126*, 107623. [CrossRef]

11. Van Maren, D.S.; van Kessel, T.; Cronin, K.; Sittoni, L. The impact of channel deepening and dredging on estuarine sediment concentration. *Cont. Shelf Res.* **2015**, *95*, 1–14. [CrossRef]
12. Lisi, I.; Feola, A.; Bruschi, A.; Pedroncini, A.; Pasquali, D.; Di Risio, M. Mathematical modeling framework of physical effects induced by sediments handling operations in marine and coastal areas. *J. Mar. Sci. Eng.* **2019**, *7*, 149. [CrossRef]
13. Borja, A.; Franco, J.; Pérez, V. A marine biotic index to establish the ecological quality of soft-bottom benthos within European estuarine and coastal environments. *Mar. Pollut. Bull.* **2000**, *40*, 1100–1114. [CrossRef]
14. Li, J.; Heap, A.D. Spatial interpolation methods applied in the environmental sciences: A review. *Environ. Model. Softw.* **2014**, *53*, 173–189. [CrossRef]
15. Elith, J.; Leathwick, J.R.; Hastie, T. A working guide to boosted regression trees. *J. Anim. Ecol.* **2008**, *77*, 802–813. [CrossRef] [PubMed]
16. Woodman, T.L.; Rueda-Uribe, C.; Henry, R.C.; Burslem, D.F.R.P.; Travis, J.M.J.; Alexander, P. Introducing LandScaleR: A novel method for spatial downscaling of land use projections. *Environ. Model. Softw.* **2023**, *169*, 105826. [CrossRef]
17. Zheng, X.; Cressie, N.; Clarke, D.A.; McGeoch, M.A. Spatial-statistical downscaling with uncertainty quantification in biodiversity modelling. *Methods Ecol. Evol.* **2025**, *16*, 837–853. [CrossRef]
18. Lomartire, S.; Marques, J.C.; Gonçalves, A.M.M. The key role of zooplankton in ecosystem services: A perspective of interaction between zooplankton and fish recruitment. *Ecol. Indic.* **2021**, *129*, 107867. [CrossRef]
19. Zhang, J.; Zhi, M.; Zhang, Y. Combined generalized additive model and random forest to evaluate the influence of environmental factors on phytoplankton biomass in a large eutrophic lake. *Ecol. Indic.* **2021**, *130*, 108082. [CrossRef]
20. Fichot, C.G.; Downing, B.D.; Bergamaschi, B.A.; Windham-Myers, L.; Marvin-DiPasquale, M.C.; Thompson, D.R.; Gierach, M.M. High-resolution remote sensing of water quality in the San Francisco Bay-Delta Estuary. *Environ. Sci. Technol.* **2016**, *50*, 573–583. [PubMed]
21. Garaba, S.P.; Zielinski, O. An assessment of water quality monitoring tools in an estuarine system. *Remote Sens. Appl. Soc. Environ.* **2015**, *2*, 1–10. [CrossRef]
22. Santos, M.; Amorim, A.; Brotas, V.; Cruz, J.P.C.; Palma, C.; Borges, C.; Favareto, L.R.; Veloso, V.; Dâmaso-Rodrigues, M.L.; Chainho, P.; et al. Spatio-temporal dynamics of phytoplankton community in a well-mixed temperate estuary. *Sci. Rep.* **2022**, *12*, 16598.
23. Cereja, R.; Chainho, P.; Brotas, V.; Cruz, J.P.C.; Sent, G.; Rodrigues, M.; Carvalho, F.; Cabral, S.; Brito, A.C. Spatial variability of physicochemical parameters and phytoplankton at the Tagus Estuary, Portugal. *Sustainability* **2022**, *14*, 13324. [CrossRef]
24. Montagna, P.A.; Palmer, T.A.; Kalke, R.D.; Gossmann, A. Suitability of using a limited number of sampling stations to represent benthic habitats in Lavaca-Colorado Estuary, Texas. *Environ. Bioindic.* **2008**, *3*, 156–171. [CrossRef]
25. Cox, T.J.S.; Maris, T.; Van Engeland, T.; Soetaert, K.; Meire, P. Critical transitions in suspended sediment dynamics in a temperate meso-tidal estuary. *Sci. Rep.* **2019**, *9*, 12745. [CrossRef] [PubMed]
26. Kang, Z.; Guo, W.; Li, J.; Zhou, B.; Wei, Q.; Nong, M. Water Quality Analysis and Evaluation in Maolingjiang River Inlet. *Adv. Mar. Sci.* **2017**, *4*, 7–16.
27. Han, X.; Pan, J.; Devlin, A.T. Remote sensing study of wetlands in the Pearl River Delta during 1995–2015 with the support vector machine method. *Front. Earth Sci.* **2018**, *12*, 521–531.
28. Avcı, C.; Budak, M.; Yağmur, N.; Balçık, F. Comparison between random forest and support vector machine algorithms for LULC classification. *Int. J. Eng. Geosci.* **2023**, *8*, 1–10. [CrossRef]
29. Lachaud, A.; Adam, M.; Mišković, I. Comparative study of random forest and support vector machine algorithms in mineral prospectivity mapping with limited training data. *Minerals* **2023**, *13*, 1073. [CrossRef]
30. *SC/T 9110-2007*; Technical Specification for Impact Assessment of Construction Projects on Marine Living Resources. China Agriculture Press: Beijing, China; Ministry of Agriculture of the People's Republic of China: Beijing, China, 2007.
31. Newcombe, C.P.; Jensen, J.O.T. Channel suspended sediment and fisheries: A synthesis for quantitative assessment of risk and impact. *N. Am. J. Fish. Manag.* **1996**, *16*, 693–727. [CrossRef]
32. Wilber, D.H.; Clarke, D.G. Biological effects of suspended sediments: A review of suspended sediment impacts on fish and shellfish with relation to dredging activities in estuaries. *N. Am. J. Fish. Manag.* **2001**, *21*, 855–875. [CrossRef]
33. Servizi, J.A.; Martens, D.W. Sublethal responses of coho salmon Oncorhynchus kisutch to suspended sediments. *Can. J. Fish. Aquat. Sci.* **1992**, *49*, 1389–1395. [CrossRef]
34. Sherk, J.A., Jr.; O'Connor, J.M.; Neumann, D.A. Effects of suspended solids on selected estuarine plankton. In *Miscellaneous Report 76-1*; U.S. Coastal Engineering Research Center: Fort Belvoir, VA, USA, 1976.
35. Arruda, J.A.; Marzolf, G.R.; Faulk, R.T. The role of suspended sediments in the nutrition of zooplankton in turbid reservoirs. *Ecology* **1983**, *64*, 1225–1235. [CrossRef]
36. Kirk, K.L.; Gilbert, J.J. Suspended clay and the population dynamics of planktonic rotifers and cladocerans. *Ecology* **1990**, *71*, 1741–1755. [CrossRef]

37. Cloern, J.E. Turbidity as a control on phytoplankton biomass and productivity in estuaries. *Cont. Shelf Res.* **1987**, *7*, 1367–1381. [CrossRef]
38. Lloyd, D.S.; Koenings, J.P.; LaPerriere, J.D. Effects of turbidity in fresh waters of Alaska. *N. Am. J. Fish. Manag.* **1987**, *7*, 18–33. [CrossRef]

Disclaimer/Publisher's Note: The statements, opinions and data contained in all publications are solely those of the individual author(s) and contributor(s) and not of MDPI and/or the editor(s). MDPI and/or the editor(s) disclaim responsibility for any injury to people or property resulting from any ideas, methods, instructions or products referred to in the content.